The Canadian Mineralogist
Vol. 44, pp. 1227-1237 (2006)

AN X-RAY- AND NEUTRON-DIFFRACTION STUDY OF SYNTHETIC FERRICOPIAPITE, $Fe_{14/3}(SO_4)_6(OD,OH)_2(D_2O,H_2O)_{20}$, AND *AB INITIO* CALCULATIONS ON THE STRUCTURE OF MAGNESIOCOPIAPITE, $MgFe_4(SO_4)_6(OH)_2(H_2O)_{20}$

JURAJ MAJZLAN[§]

Institute of Mineralogy and Geochemistry, Albert-Ludwig University of Freiburg, Albertstraße 23b, D-79104 Freiburg, Germany

BORIS KIEFER

Department of Physics, 153 Gardiner Hall, New Mexico State University, Las Cruces 88003, New Mexico, USA

ABSTRACT

We determined the positions of all atoms, including the light ones (D, H), in the crystal structure of synthetic ferricopiapite $Fe_{14/3}(SO_4)_6(OD,OH)_2(D_2O,H_2O)_{20}$, using X-ray synchrotron [λ 0.64905(1) Å] and neutron (λ 2.0787 Å) powder diffraction. The H/(H + D) ratio in the sample is 0.09, as determined by infrared spectroscopy. The results of the diffraction study are supported by *ab initio* calculations of the structure of magnesiocopiapite, $MgFe_4(SO_4)_6(OH)_2(H_2O)_{20}$. Neutron-diffraction data were collected at both room and low (~16 K) temperature. The X-ray-diffraction pattern was collected at room temperature only. The room-temperature diffraction data (X-ray and neutron) were refined simultaneously. The structural model was refined in space group $P\bar{1}$, with unit-cell parameters *a* 7.3926(1), *b* 18.3806(1), *c* 7.3361(1) Å, α 93.933(1), β 102.212(1) and γ 98.900(1)° (XRD data). Positions of the heavy atoms determined in this study are virtually identical to those determined in the earlier studies of the structure of copiapite. The structure consists of infinite heteropolyhedral chains parallel to [101] and isolated $[A(D_2O)_6]$ sites. The occupancy of the isolated *A* site in our ferricopiapite sample is 0.63(1). According to an analysis of the hydrogen-bonding network, the infinite chains in the structure have the composition $[Fe_4(SO_4)_6(D_2O)_8(OD)_2](D_2O)_2$. The isolated sites form slabs of composition $\{[A(D_2O)_6](D_2O)_4\}$ with isolated D_2O molecules attached to the infinite chains *via* a complicated set of hydrogen bonds. *Ab initio* calculations provide insight into the bonding around the isolated *A* site, where occupied by a cation (Mg^{2+}) and where vacant. The octahedral coordination of the *A* site is preserved whether the site is occupied or vacant. However, vacating the site results into a 17% increase of the volume of the octahedron and significant re-arrangement of the ligands. *Ab initio* calculations also suggest that the high-spin state of Fe^{3+} in copiapite is the stable electronic configuration.

Keywords: ferricopiapite, magnesiocopiapite, crystal structure, hydrogen bonding, X-ray diffraction, neutron diffraction, *ab initio* calculations.

SOMMAIRE

Nous avons déterminé la position de tous les atomes, y inclus les atomes légers (D, H), dans la structure cristalline de la ferricopiapite $Fe_{14/3}(SO_4)_6(OD,OH)_2(D_2O,H_2O)_{20}$, au moyen de diffraction X avec rayonnement synchrotron [λ 0.64905(1) Å] et diffraction de neutrons (λ 2.0787 Å) sur poudre. Le rapport H/(H + D) dans l'échantillon est 0.09, comme l'indique la spectroscopie infra-rouge. Les résultats de l'étude par diffractométrie sont étayés par des calculs *ab initio* de la structure de la magnésiocopiapite, $MgFe_4(SO_4)_6(OH)_2(H_2O)_{20}$. Les données de diffraction neutronique ont été prélevées à température ambiante et à environ ~16 K. Le spectre de diffraction X a été prélevé à température ambiante seulement. Les données prélevées à température ambiante (diffraction X et diffraction de neutrons) ont été affinées ensemble. Le modèle structural a été affiné dans le groupe d'espace $P\bar{1}$, pour donner les paramètres réticulaires *a* 7.3926(1), *b* 18.3806(1), *c* 7.3361(1) Å, α 93.933(1), β 102.212(1) et γ 98.900(1)° (données en diffarction X). Les positions des atomes lourds sont essentiellement identiques à celles des études antérieures de la structure de la copiapite. La structure est faite de chaînes infinies hétéropolyédriques parallèles à [101] et des sites isolés $[A(D_2O)_6]$. L'occupation du site isolé *A* est 0.63(1) dans notre échantillon de ferricopiapite. Selon une analyse du réseau de liaisons hydrogène, les chaînes infinies du réseau auraient la composition $[Fe_4(SO_4)_6(D_2O)_8(OD)_2](D_2O)_2$. Les sites isolés forment des plaques de composition $\{[A(D_2O)_6](D_2O)_4\}$ ayant des molécules D_2O isolées rattachées aux chaînes infinies *via* un réseau complexe de liaisons hydrogène. Les calculs *ab initio* fournissent une indication des liaisons autour du site isolé *A*, où celui-ci est occupé par un cation (Mg^{2+}) et où il est vacant. La coordinence octaédrique du site *A* est conservée

§ *E-mail address*: juraj.majzlan@minpet.uni-freiburg.de

quel que soit le taux d'occupation du site. Toutefois, un site vacant mène à une augmentation de 17% du volume de l'octaèdre et une réorganisation importante des ligands. D'après les calculs *ab initio*, l'état de spin élevé de Fe^{3+} serait la configuration électronique stable dans la copiapite.

(Traduit par la Rédaction)

Mots-clés: ferricopiapite, magnésiocopiapite, structure cristalline, liaisons hydrogène, diffraction X, diffraction neutronique, calculs *ab initio*.

Introduction

Copiapite is one of the minerals precipitating from acid mine-drainage (AMD) waters (*e.g.,* Jamieson *et al*. 2005). This mineral is associated with other Fe^{3+} sulfates, such as jarosite [$KFe_3(SO_4)_2(OH)_6$], rhomboclase [$(H_5O_2)Fe(SO_4)_2(H_2O)_2$], or coquimbite [$Fe_2(SO_4)_3(H_2O)_9$]. AMD minerals incorporate and store a variety of metals that originate by weathering of pyrite and the attack of acidic solutions on the ambient minerals and rocks. Minerals of the copiapite group display a remarkably wide range of compositional variations (Atencio *et al*. 1996). The general formula of these minerals is $A{Fe^{3+}}_4(SO_4)_6(OH)_2(H_2O)_{20}$, where *A* = Fe^{2+} (copiapite *sensu stricto*), Mg^{2+} (magnesiocopiapite), Cu^{2+} (cuprocopiapite), Ca^{2+} (calciocopiapite), Zn^{2+} (zincocopiapite), $2/3Fe^{3+}$ (ferricopiapite), and $2/3Al^{3+}$ (aluminocopiapite). The crystal structure of this group of minerals was solved by Süsse (1972) for magnesiocopiapite, and by Fanfani *et al*. (1973) for ferricopiapite.

In this study, we investigated the structure of synthetic, deuterated ferricopiapite by powder synchrotron X-ray and neutron diffraction in order to determine the position of the light atoms (D, H). The experimental part of the work is complemented by *ab initio* calculations on the structure of magnesiocopiapite. The structure of magnesiocopiapite was preferred over that of ferricopiapite in the *ab initio* work because the vacancies in the latter caused additional complications. As will be shown, only the combination of experiments and theory gave a clear picture of the location and behavior of light atoms in this complicated structure.

The Crystal Structure of Copiapite

The backbone of the copiapite structure consists of infinite chains of composition $[Fe_4(SO_4)_6(H_2O)_8(OH)_2]$ parallel to [101] (Fig. 1). The cation at the *A* site is octahedrally coordinated by H_2O molecules, forming $[A(H_2O)_6]$ units (Fig. 1), and connected to the rest of the structure only by hydrogen bonds. There are six isolated H_2O molecules in the unit cell. The two structural models (Süsse 1972, Fanfani *et al*. 1973) are slightly different, especially in the tilting of the infinite chains of polyhedra along [101]. Fanfani *et al*. (1973) provided a guess for a likely hydrogen-bond scheme in the structure of ferricopiapite. However, the positions of the hydrogen atoms remained unknown.

Materials and Methods

The sample of deuterated ferricopiapite was synthesized from a mixture of 12.3 g of $Fe_2(SO_4)_3(H_2O)_{\sim 6.75}$ [labeled as $Fe_2(SO_4)_3{\bullet}XH_2O$, reagent grade, Alfa Aesar) and 6 mL of D_2O (99.9 at.% D, Aldrich]. The $Fe_2(SO_4)_3(H_2O)_{\sim 6.75}$ is a very fine-grained, strongly hygroscopic material that is amorphous to X-rays. This material was dehydrated in a sintered alumina crucible by heating at 100°C for 1 hour, at 160°C overnight, and at 500°C for one hour. The dehydrated powder was

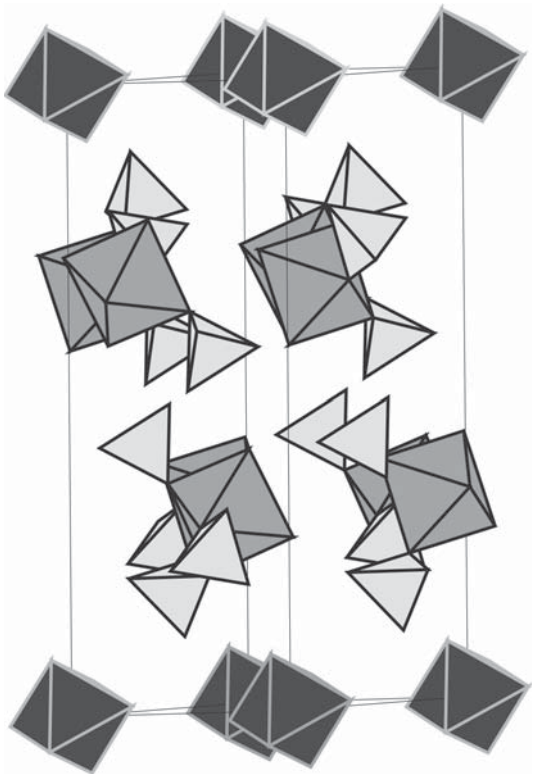

FIG. 1. A schematic representation of the structure of ferricopiapite. The infinite chains are almost perpendicular to the plane of the projection. The sulfate tetrahedra are light grey and the $Fe(O,OH,OH_2)_6$ octahedra are medium grey. The $[A(H_2O)_6]$ sites are shown as dark octahedra. Hydrogen atoms and isolated H_2O molecules are not shown for clarity. Unit-cell edges are outlined by thin solid lines.

allowed to cool to ~100°C, and then mixed with D_2O in a polyethylene vial. The vial was sealed, isolated with a teflon tape, and placed in an oven at 50°C. The light beige slurry turned to a dense, viscous brown liquid in two days. In another two days, the viscous, honey-like liquid recrystallized into a compact aggregate of yellow ferricopiapite.

The synchrotron XRD pattern was collected nine days after the sample crystallized. The XRD pattern was collected at the bending magnet beamline X3B1 at National Synchrotron Light Source (Brookhaven National Laboratory). X-rays of a wavelength 0.64905(1) Å were selected with a double crystal Si(111) monochromator. The wavelength and the zero angle of the diffractometer were determined with a NIST 1976 standard reference material (corundum, α–Al_2O_3). The sample was loaded in air into a glass capillary (1.0 mm in outer diameter) that was rotated about its axis during the data collection. The intensity of the incoming beam was monitored during the data collection with an ion chamber, and the measured intensities of the diffracted beam were corrected for the decay and fluctuations of the primary beam. The diffracted beam was analyzed with a Ge(111) crystal and Na(Tl)I scintillation detector. The XRD pattern was collected at room temperature, over an angular range of 1.5 to 37.0° 2θ, with step size of 0.002°, and counting time of 1 s per step.

The neutron powder-diffraction pattern was collected two days after the sample crystallized, on the BT–1 diffractometer at the Center for Neutron Research at the National Institute of Standards and Technology, using a Ge(311) monochromator with a 75° take-off angle and a 15' in-pile Soller collimator. The sample was loaded in a vanadium sample container, 50 mm long, 15.6 mm in diameter, under a stream of dry He in an open glove-box. Relative humidity during loading was ≤15%. The vanadium container was sealed by pressing on an indium seal. The sample was then exposed to a beam of neutrons with λ = 2.0787 Å. The diffracted neutrons were detected by an array of 32^3 He detectors at 5° intervals. The diffraction pattern was collected over a 2θ range of 1.3 – 166.3° with a step size of 0.05° at both room temperature and ~16 K. A closed-cycle He refrigerator was used for the temperature control at low temperature.

The FTIR spectra were collected with a Bruker IFS 66 v/s Fourier transform infrared (FTIR) spectrometer in attenuated total reflectance (ATR) mode. The sample was pressed against a single-reflection diamond crystal, and the signal was recorded with a DTGS detector.

The neutron and X-ray measurements were augmented by *ab initio* calculations that are based on density-functional theory (DFT, Hohenberg & Kohn 1964). These calculations make no assumptions on the nature of bonding and can provide information that cannot be extracted from the experimental data. We used the PAW method (Blöchl 1994, Kresse & Joubert 1999) as implemented in the VASP code (Vienna *ab initio* software package) (Kresse & Hafner 1993, Kresse & Furthmüller 1996a, b). The results of this approach have been shown to be of comparable accuracy to all electron calculations (Kresse & Joubert 1999). Copiapite comprises different types of bonds that range from ionic-covalent bonding among the heavier ions to hydrogen bonding of the OH^- and H_2O groups. It is to be expected that charge density changes rapidly in the vicinity of the OH^- groups and the H_2O molecules. Therefore, we used the generalized-gradient approximation (GGA) in the parametrization of Perdew, Burke and Enzerhof (PBE; Perdew *et al*. 1996), which accounts explicitly for charge-density gradients. Tests showed that converged solutions to the Kohn–Sham equations (Kohn & Sham 1965) could be obtained for E_{cut} = 500 eV and one *k*-point (zone center; Γ-point). These computational parameters were adopted for all calculations presented here and lead to total energies that converged to within 4 meV/atom, and Pulay stresses due to the incompleteness of the basis set that were less than 0.02 GPa. All structural parameters (cell shape and internal coordinates) were relaxed simultaneously to find the static ground-state structure at zero pressure. In order to address the spin structure of ferricopiapite, we consider iron in its high-spin form (five unpaired electrons) and in its low-spin state (one unpaired electron).

Partially occupied sites, such as in the case of ferricopiapite, provide a challenge for computations. A common remediation of this problem is the use of supercells. In the present case of ferricopiapite, the *A* site is 2/3 occupied and 1/3 vacant. The smallest possible supercell that can be used to simulate the structure of ferricopiapite requires $3 \times 99 = 297$ atoms. However, such supercells only represent a perfectly ordered superstructure. Many other vacancy-ordering schemes are possible; they would require even larger supercells, each with a different total energy. Moreover, vacating 1/3 of the *A* sites will lower the symmetry from $P\bar{1}$ to $P1$, inconsistent with experimental observations. For these reasons, we chose a different approach in the computations: we consider magnesiocopiapite, where the *A* site is completely occupied by Mg^{2+} or completely vacant in order to assess differences in the hydrogen bonding scheme. Whereas the $Mg^{2+} \rightleftharpoons Fe^{3+}$ substitution affects the local charge-balance, it is expected that the spherical charge-density of Mg^{2+} is similar to the spherical charge-density of high-spin ferric iron with a half-filled 3*d* electronic shell. The differences in charges of Mg^{2+} and Fe^{3+} may cause shorter bond-length for Fe^{3+} and oxygen. However, Mg^{2+} is a smaller cation, and the size dissimilarity may at least partly compensate for the effects due to charge difference. For the simulation of the vacant *A* site, the entire Mg atom, *i.e*., Mg^{2+} and two electrons, was removed. The charge balance of the entire structure was thereby preserved. The comparison of the relaxed structures with the results of X-ray- and neutron-diffraction refinements will therefore allow us

to assess the sensitivity of the coordination of the *A* site to the local charge.

Results

The sample was found to exchange deuterium for hydrogen rapidly, either in contact with ambient humidity or commonly used laboratory liquids, such as methanol or ethanol. An FTIR spectrum indicated that the ratio H/(H + D) in the freshly prepared sample is about 0.09. After a 24-hour exposure to air, almost all deuterium was exchanged for hydrogen. Washing with ethanol resulted into immediate exchange of most deuterium for hydrogen. Because of this, the sample was not washed at all, and stored in a secondary vial sealed in a dry atmosphere.

The sample consisted mostly of ferricopiapite but also contained a minor proportion of interstitial liquid. The liquid could not be removed, because washing would make the sample unusable for neutron diffraction. On the other hand, the interstitial liquid slowly crystallized to rhomboclase at room temperature, thus adding a crystalline impurity to the sample. The fraction of this rhomboclase impurity increased with time; although the sample was phase-pure for the neutron-diffraction experiment, additional rhomboclase was present during the collection of XRD data.

Refinement of the positions of the heavy atoms

All structural models were refined with GSAS (Larson & von Dreele 1994). The synchrotron XRD pattern was used for the refinement of the atom positions of the heavy atoms. The starting values for the cell parameters, atom positions, and displacement factors for ferricopiapite and rhomboclase were taken from our previous work on these phases (Majzlan *et al*. 2006). Among the crystalline phases, 89.6 wt.% was ferricopiapite and 10.4% rhomboclase. The background was modeled by the Chebyshev polynomial in GSAS with 18 terms. Peak profile was modeled by a pseudo-Voigt function (Thompson *et al*. 1987) with the asymmetry correction (Finger *et al*. 1994). The zero point of the diffractometer was refined in the early stages and then kept constant. An absorption correction was modeled using the Hewat function in GSAS, with the absorption coefficient fixed at a value derived from the chemical composition, calculated density of the sample, and an assumed 50% packing fraction. For rhomboclase, only the unit-cell parameters and position of S were refined; Fe lies on a special position (0, 0, 0), and the positions of the oxygen atoms were not refined because of small fraction of this phase in the sample. The data for rhomboclase were kept constant in the later phases of the refinement. For ferricopiapite, we refined the positions of all Fe, S, and O atoms, along with occupancy of the *A* site. Isotropic displacement factors were constrained to be identical for all atoms of the same element, and refined. Soft restraints were placed on the S–O bond distances (S–O distance = 1.47 ± 0.03 Å). A total of 97 variables (Fe, S, O atom positions, *A*-site occupancy, unit-cell parameters, profile coefficients, scale factor) were refined in the last stable cycle.

Low-temperature neutron diffraction

The temperature during the data collection fluctuated between 15.57 and 19.21 K. There were only ferricopiapite peaks, with no evidence of an additional phase. The model for heavy atoms (Fe, S, and O), refined from the XRD data, was transferred to the neutron-pattern refinement, and used without further refinement. A starting model for the light atoms was created with no consideration of possible hydrogen-bonding schemes. The deuterium atoms were placed 1.00 Å from their oxygen atoms, with a 109° D–O–D angle for the D_2O molecules. In the initial stages of refinement, the deuterium atoms were allowed to drift freely with significant damping. No deuterium atom drifted away from its oxygen atom, although some of the new positions were found to be unreasonable. In such cases, these deuterium atoms were re-assigned the initial positions, and allowed to drift again. The refinement of the deuterium positions alternated with refinement of the peak-profile parameters, background coefficient, and unit-cell parameters. The background was modeled by a cosine Fourier series function with 21 coefficients, the peak profiles by a Gaussian function. Soft restraints were placed on the O–D bond lengths and D–O–D bond angles (bond distance O–D = 0.99 ± 0.03 Å, bond angle O–D–O = 109.5 ± 0.5°). The unit-cell parameters for ferricopiapite at low temperature are listed in Table 1. The positions and displacement factors of all atoms are given in Table S1 (supplementary material), available from the Depository of Unpublished Data, CISTI, National Research Council of Canada, Ottawa, Ontario, K1A 0S2, Canada, and also from the electronic crystal-structure database at http://www.minsocam.org/MSA/Crystal_Database.html.

Room-temperature neutron-diffraction and synchrotron XRD refinements

The positions of the heavy atoms and deuterium, obtained from refinement of the XRD and low-temperature neutron data, respectively, were used as a starting model for a simultaneous refinement of the XRD and room-temperature neutron data (Figs. 2, 3). The functions used to model background, peak shape, *etc*., for both sets of data are the same as described above. The refinement included three phases: two ferricopiapite phases and rhomboclase. A separate ferricopiapite phase was used for XRD and for neutron data because of slight mismatch among the unit-cell parameters obtained by the two methods (Table 1). The mismatch is likely due to temperature difference between the

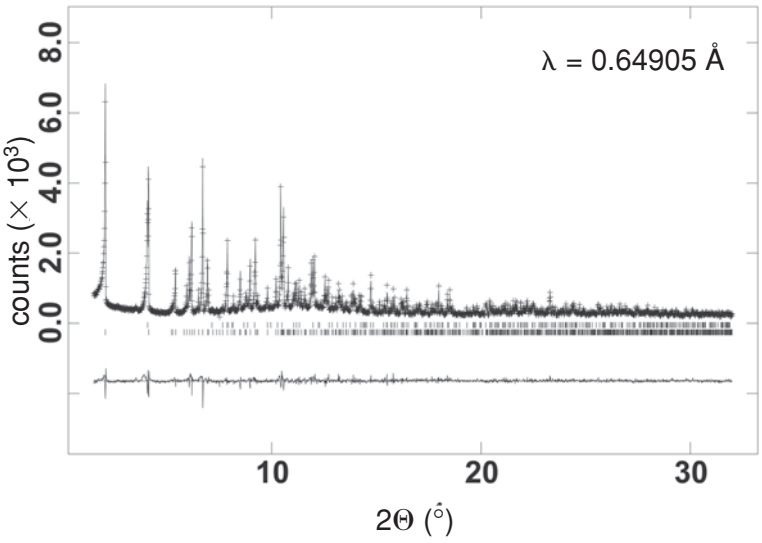

FIG. 2. Synchrotron X-ray-diffraction pattern (taken at room temperature) of the mixture of ferricopiapite and rhomboclase, with the calculated and difference plot from the Rietveld refinement. The upper row of tickmarks shows the calculated position of rhomboclase peaks, the lower row, the position of ferricopiapite peaks.

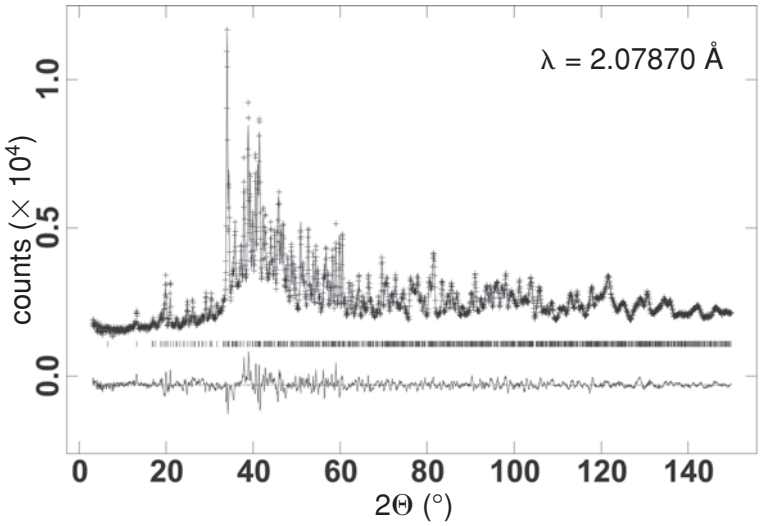

FIG. 3. Neutron-diffraction pattern (taken at room temperature) of ferricopiapite with the calculated and difference plot from the Rietveld refinement.

"room temperature" at the NSLS synchrotron and NIST neutron source. Another source of the difference in unit-cell parameters may be the different H:D ratio in the ferricopiapite phase during the collection of X-ray and neutron powder-diffraction data. The atom positions and displacement factors were constrained to be identical for the two ferricopiapite phases. Positions of heavy and light atoms were allowed to vary at the different stages of the refinement. However, the changes in the positions of the heavy atoms were insignificant. No parameters of the rhomboclase phase were allowed to vary. Results of this refinement are summarized in Tables 1 and 2, and the experimental and calculated X-ray- and neutron-diffraction patterns are compared in Figures 2 and 3, respectively. Altogether, 98 variables (atom positions and displacement factors for D atoms, unit-cell parameters for the two ferricopiapite phases, scale factors) were refined in the last stable cycle.

TABLE 1. STATISTICS OF RIETVELD REFINEMENT AND STRUCTURAL DATA FOR FERRICOPIAPITE, $Fe_{14+3}(SO_4)_6(OD)_2(D_2O)_{20}$, AND RHOMBOCLASE, $(D_5O_2)Fe(SO_4)_2(D_2O)_2$

results of diffraction experiments	room temperature*			low temperature†
χ^2	2.83			5.89
wR_p	0.0610			0.0451
R_p	0.0452			0.0380
wR_p – background	0.0855			0.0507
R_p – background	0.0562			0.0407
phase	ferricopiapite (XRD data)	ferricopiapite (neutron data)	rhomboclase	ferricopiapite
space group	$P\bar{1}$	$P\bar{1}$	*Pnma*	$P\bar{1}$
Z	1	1	4	1
lattice parameters				
a (Å)	7.3926(1)	7.3968(3)	9.7245(4)	7.3682(3)
b (Å)	18.3806(1)	18.3924(7)	18.292(1)	18.2626(7)
c (Å)	7.3361(1)	7.3400(3)	5.4289(2)	7.3014(3)
α (°)	93.933(1)	93.964(3)		93.533(4)
β (°)	102.212(1)	102.223(4)		102.150(4)
γ (°)	98.900(1)	98.892(3)		98.773(3)
cell volume (Å^3)	957.23(1)	958.83(6)	965.7(1)	944.78(6)
ab initio calculations	HS, *A* occupied‡	HS, *A* vacant§		
lattice parameters				
a (Å)	7.5515	7.4967		
b (Å)	18.601	19.019		
c (Å)	7.4460	7.4000		
α (°)	95.49	96.33		
β (°)	102.71	103.19		
γ (°)	98.71	99.77		
cell volume (Å^3)	999.46	1000.08		

* Combined XRD and neutron-diffraction refinement; atom positions in Table 2. † Neutron-diffraction refinement; atom positions in Table S1 (supplementary material, deposited). ‡ Atom positions in Table 3. § Atom positions in Table S2 (supplementary material, deposited). The lattice parameters from the *ab initio* calculations are presented for high-spin (HS) state of Fe^{3+}, with the *A* site either occupied or vacant.

Ab initio calculations of the structure of magnesiocopiapite, $MgFe^{3+}_4(SO_4)_6(OH)_2(H_2O)_{20}$

The *ab initio* calculations were started from a model very similar to the initial model used for low-temperature neutron diffraction (see above). The only modification of this initial model was the introduction of Mg^{2+} at the *A* site. The atom positions for the optimized model are listed in Table 3. The GGA calculations show that the high-spin (HS) structure is energetically more favorable than the low-spin (LS) state by 1.7 eV/unit

TABLE 2. FRACTIONAL POSITIONS AND DISPLACEMENT FACTORS FOR ATOMS IN THE FERRICOPIAPITE STRUCTURE AT ROOM TEMPERATURE

atom	*x*	*y*	*z*	U_{iso}*100
Fe*A*	0	0	0	1.5(4)
Fe1	0.7871(6)	0.3154(2)	0.5507(5)	1.4(1)
Fe2	0.5950(5)	0.6695(2)	0.8052(5)	1.5(1)
S1	0.8291(10)	0.7351(4)	0.2189(11)	3.0(3)
S2	0.8197(10)	0.4189(4)	0.2232(10)	1.8(3)
S3	0.6405(10)	0.1948(4)	0.1988(10)	3.1(3)
O1	0.736(2)	0.6698(6)	0.081(2)	2.9(6)
O2	0.691(1)	0.7671(6)	0.305(2)	0.7(5)
O3	0.047(2)	0.2939(6)	0.625(2)	4.3(7)
O4	0.056(2)	0.2062(6)	0.852(2)	1.6(6)
O5	0.628(1)	0.3921(6)	0.110(2)	0.8(5)
O6	0.846(2)	0.4923(5)	0.335(2)	2.7(6)
O7	0.880(2)	0.3614(6)	0.336(2)	0.8(5)
O8	0.936(2)	0.4215(6)	0.084(2)	2.5(6)
O9	0.560(2)	0.1156(5)	0.174(2)	1.4(5)
O10	0.510(1)	0.7602(5)	0.866(2)	0.4(5)
O11	0.788(2)	0.2130(6)	0.093(2)	2.4(6)
O12	0.726(2)	0.2190(7)	0.400(1)	3.1(6)
O13H	0.459(2)	0.6623(6)	0.539(2)	1.4(5)
O14w	0.695(2)	0.2725(7)	0.757(2)	3.7(7)
O15w	0.859(2)	0.4113(6)	0.726(2)	1.2(6)
O16w	0.232(3)	0.9478(10)	0.085(3)	13.4(10)
O17w	0.692(2)	0.5723(6)	0.760(2)	2.0(6)
O18w	0.050(3)	0.9839(11)	0.735(3)	15.4(11)
O19w	0.830(2)	0.7298(6)	0.742(2)	3.3(6)
O20w	0.178(3)	0.0917(10)	0.049(3)	10.6(9)
O21w	0.770(2)	0.9100(7)	0.446(2)	7.6(8)
O22w	0.534(2)	0.5597(6)	0.286(2)	2.4(6)
O23w	0.643(2)	0.0740(7)	0.565(2)	11.0(9)
D1 (O13)	0.495(2)	0.6263(6)	0.458(2)	0.1(3)
D2 (O14)	0.746(2)	0.2537(7)	0.873(2)	1.5(4)
D3 (O14)	0.557(1)	0.2612(8)	0.743(2)	0.9(4)
D4 (O15)	0.900(3)	0.4147(10)	0.864(2)	6.1(7)
D5 (O15)	0.953(2)	0.4470(7)	0.683(2)	1.8(4)
D6 (O16)	0.293(3)	0.9357(14)	0.216(2)	12.4(11)
D7 (O16)	0.302(3)	0.9442(17)	-0.018(3)	15.9(13)
D8 (O17)	0.828(1)	0.5710(7)	0.809(2)	1.2(4)
D9 (O17)	0.622(2)	0.5218(6)	0.750(2)	1.7(5)
D10 (O18)	0.113(4)	1.0252(14)	0.681(4)	22.5(20)
D11 (O18)	-0.074(2)	0.9576(13)	0.646(3)	9.9(9)
D12 (O19)	0.838(3)	0.7200(11)	0.611(2)	5.4(7)
D13 (O19)	0.952(2)	0.7492(9)	0.817(2)	3.5(6)
D14 (O20)	0.314(2)	0.0983(14)	0.107(4)	16.4(13)
D15 (O20)	0.152(3)	0.1366(8)	-0.011(3)	8.3(8)
D16 (O21)	0.675(3)	0.9383(13)	0.401(4)	10.9(10)
D17 (O21)	0.750(3)	0.8609(7)	0.377(2)	6.4(7)
D18 (O22)	0.659(2)	0.5453(13)	0.309(3)	8.7(9)
D19 (O22)	0.506(2)	0.5828(9)	0.168(2)	3.6(5)
D20 (O23)	0.506(2)	0.0727(17)	0.542(6)	20.4(17)
D21 (O23)	0.714(3)	0.1228(9)	0.551(4)	14.5(14)

These data were obtained by refinement of the structural model with the room-temperature neutron-diffraction pattern and the synchrotron X-ray-diffraction pattern. The occupancy of the isolated *A* site (Fe*A*) is 0.633(9); occupancies of other sites are 1.00.

cell. The finding that the HS state is the more stable at ambient conditions is consistent with observations in other ferric oxides at ambient pressure, such as hematite and goethite (Burns 1993). The calculated zero-pressure volume is 999.5 Å^3, ~5.8% larger than the volume obtained from the low-temperature neutron-scattering data. An overestimation of the cell volume is not uncommon for the GGA and has been observed previously in other systems, such as $Mg_3Si_4O_{10}(OH)_2$ (4.8%, Stixrude 2002). The lattice parameters *a*, *b*, and *c* in the HS calculations are overestimated by 2.5, 1.9, and 2.0%, respectively, as compared to the low-temperature neutron-scattering results. The angles α, β, and γ agree with the low-temperature neutron-scattering results to within 2.1, 0.6, and 0.1%, respectively.

The unit-cell volume is rather sensitive to the spin state of iron. Changing the spin state of iron from HS to LS reduces the volume by ~4.6%. This reduced volume is consistent with the ionic radii for Fe^{3+}(LS) and Fe^{3+}(HS), 0.55 Å and 0.645 Å, respectively (Shannon 1976). Thus changing the spin-state of iron from HS to LS leads to a decrease the ionic radius of iron by $[Fe^{3+}(HS) - Fe^{3+}(LS)] / Fe^{3+}(HS) \approx 14.7\%$. The associated shortening of the average bond-length for Fe(2) and Fe(3) are ~3.9% and ~4.4%, respectively. The mismatch between ionic size difference and cell-volume difference may be explained by the geometrical constraints due to the three coordinating SO_4^{2-} tetrahedra of the Fe(2) and Fe(3) sites. The coulombic repulsion between the S^{6+} cations in the neighboring tetrahedra may prevent a strong contraction of the Fe–O bonds.

For the calculations of the case with a vacant *A* site, we find that the HS state is stabilized by ~0.9 eV/unit cell as compared to the structure with ferric iron in its LS state. The comparison of the ground-state structures shows that removing Mg from the *A* site leads to a marginal increase of the unit-cell volume by 0.06% (Table 1). Changing the spin state of ferric iron from HS to LS reduces the average Fe–O bond length by ~4.4%, a value that compares well with the calculations for a fully occupied *A* site. The chains along [101] are thus largely unaffected by the occupancy of the *A* site. The largest changes are associated with the arrangement of the H_2O molecules in the magnesiocopiapite structure. Atom positions of the calculations with the *A* site vacant are given in Table S2 (supplementary material), available from the Depository of Unpublished Data, CISTI, Ottawa, Ontario, K1A 0S2, Canada, and also from the electronic crystal-structure database at http://www.minsocam.org/MSA/Crystal_Database.html.

TABLE 3. FRACTIONAL POSITIONS OF ATOMS IN THE STRUCTURE OF MAGNESIOCOPIAPITE

atom	*x*	*y*	*z*	atom	*x*	*y*	*z*
Mg*A*	0.0000	0.0000	0.0000	O20	0.1595	0.1012	0.0446
Fe1	0.7836	0.3157	0.5376	O21	0.7558	0.9231	0.4343
Fe2	0.6077	0.6695	0.8163	O22	0.5139	0.5566	0.2777
S1	0.8382	0.7405	0.2361	O23	0.5966	0.0801	0.5477
S2	0.8059	0.4207	0.2086	H1 (O13)	0.4954	0.6221	0.4641
S3	0.6299	0.1921	0.1771	H2 (O14)	0.2597	0.7512	0.1468
O1	0.7549	0.6773	0.0812	H3 (O14)	0.4536	0.7387	0.2660
O2	0.6913	0.7694	0.3067	H4 (O15)	0.1086	0.5869	0.1523
O3	0.0488	0.2915	0.6072	H5 (O15)	0.0131	0.5541	0.3082
O4	0.0427	0.2029	0.8290	H6 (O16)	0.2208	0.8973	0.0229
O5	0.6095	0.3955	0.0995	H7 (O16)	0.3514	0.9729	0.0723
O6	0.8230	0.4928	0.3208	H8 (O17)	0.1650	0.4265	0.1880
O7	0.8619	0.3643	0.3318	H9 (O17)	0.3709	0.4759	0.2558
O8	0.9304	0.4260	0.0804	H10 (O18)	0.8823	0.9822	0.3193
O9	0.5299	0.1163	0.1457	H11 (O18)	0.0697	0.0419	0.3717
O10	0.5024	0.7573	0.8859	H12 (O19)	0.1451	0.2796	0.3835
O11	0.7777	0.1995	0.0733	H13 (O19)	0.0428	0.2503	0.1741
O12	0.7133	0.2141	0.3828	H14 (O20)	0.2955	0.1103	0.0886
O13	0.4671	0.6593	0.5547	H15 (O20)	0.1275	0.1390	0.9643
O14	0.6826	0.2754	0.7538	H16 (O21)	0.6272	0.9274	0.4448
O15	0.8785	0.4122	0.7113	H17 (O21)	0.7478	0.8705	0.3939
O16	0.2359	0.9472	0.0913	H18 (O22)	0.6356	0.5405	0.2943
O17	0.7046	0.5743	0.7514	H19 (O22)	0.4928	0.5773	0.1597
O18	0.0331	0.9841	0.7333	H20 (O23)	0.6787	0.0735	0.6649
O19	0.8361	0.7282	0.7434	H21 (O23)	0.6542	0.1239	0.5051

These data are the result of *ab initio* calculations. The *A* site is fully occupied by Mg^{2+}. Fe^{3+} is in high-spin state. Uncertainties are estimated to be less than ±0.002 for Fe, and O and ±0.003 for S, and H. Mg is fixed by symmetry.

Discussion

The positions of the heavy atoms (Table 2), determined in the synchrotron XRD refinement, do not diverge significantly from the results of Fanfani *et al.* (1973). The principal features of the copiapite structure (Fig. 1) are preserved. The bond distances among the heavy atoms in ferricopiapite are listed in Table 4 and compared to those obtained by *ab initio* calculations for magnesiocopiapite. The hydrogen-bonding scheme, obtained by the free drift of deuterium atoms, was found to be very close to the one proposed by Fanfani *et al.* (1973). Bond distances and angles for the bonds among O and D atoms in ferricopiapite or O and H atoms in magnesiocopiapite are listed in Table 5. Bond-valence analysis (Table S3, supplementary material) gave values approximately equal to formal charges for all atoms in the structure.

Occupancy of all atoms except ^{A}Fe was kept at 1.00 in the final refinement. The refined value, 0.626(6) (low-temperature data) and 0.633(9) (room-temperature data) for ^{A}Fe, is almost equal to the theoretical 2/3 occupancy. Majzlan *et al.* (2006) also found lower than 2/3 occupancy on this site for hydrogen-containing ferricopiapite. It is not clear whether the value slightly lower than 2/3 is an experimental artifact or another complexity of the structure of this phase. Variation of occupancies of all other sites atoms gave values close to 1.0, confirming that they are fully occupied.

The refinement of displacement factors gives clues about sites with significant disorder in the structure of ferricopiapite. Whereas the displacement factors of all atoms within the infinite chains have reasonable and small values, displacement factors of the oxygen atoms coordinating the *A* site and some isolated H_2O molecules are relatively large (Table 2). Therefore, at

least some displacement factors do not describe the magnitude of vibration of the atoms, but the degree of static disorder in the structure. It is a common practice to attempt a refinement involving split sites for atoms with such high displacement-factors. Our effort to create split sites did not yield a physically reasonable structural environment, for reasons that we fail to understand. The complexity of the structure and the constraints already placed on the bond distances and angles suggest that the final refinement provides an "average" structure of these sites, and the detailed questions about disordered sites should be addressed by the *ab initio* calculations.

Hydrogen bonding

Data describing the hydrogen bonds within the ferricopiapite structure are summarized in Table 6. Most hydrogen bonds found in the structure of ferricopiapite fall in the category of weak hydrogen bonds, with the distance between the two oxygen atoms [d(O…O)] greater than 2.70 Å (Libowitzky & Beran 2004). Only one of them (O15w–D4–O8) falls in the range of strong hydrogen bonds [2.50 Å < d(O…O) < 2.70 Å, Libowitzky & Beran 2004]. The oxygen of the isolated D_2O molecule O22w is the acceptor oxygen for the hydrogen bond from D13, the only hydroxyl in the structure. It also accepts a hydrogen bond from D9, one of the deuterium atoms on O17. This isolated D_2O molecule forms two hydrogen bonds to O5 and O6, two atoms coordinating S2. The D_2O22w is therefore a structural component of the infinite chains, providing the necessary hydrogen bonding to the hydroxyl O13D1. The infinite chains including the D_2O22w molecule form units with composition $[Fe_4(SO_4)_6(D_2O)_8(OD)_2](D_2O)_2$. The octahedra $[A(D_2O)_6]$ and isolated D_2O molecules O21w and O23w form slabs of composition $\{[A(D_2O)_6](D_2O)_4\}$. The site *A* is only 2/3 filled by Fe^{3+}, and coordinated by O16w, O18w, and O20w. The oxygen atoms O18w form hydrogen bonds to O21w, linking the adjacent $[A(D_2O)_6]$ octahedra (Fig. 4a). The oxygen atoms O20w form hydrogen bonds to O4 and O9, connecting the $[A(D_2O)_6]$ octahedra to the infinite chains. The oxygen atoms O16w form hydrogen bonds to the isolated D_2O molecules O23w and to O9, an oxygen atom in the infinite chains.

Our *ab initio* calculations provide an alternative scheme for the hydrogen bonding within the slabs

TABLE 4. BOND DISTANCES FOR HEAVY ATOMS IN FERRICOPIAPITE* AND MAGNESIOCOPIAPITE§

ferricopiapite		magnesiocopiapite	
A – *B*	distance (Å)	*A* – *B*	distance (Å)
Fe*A* – O20w	1.93(2)	Mg*A* – O20	2.03
Fe*A* – O20w	1.93(2)	Mg*A* – O20	2.03
Fe*A* – O18w	2.06(2)	Mg*A* – O18	2.06
Fe*A* – O18w	2.06(2)	Mg*A* – O18	2.06
Fe*A* – O16w	2.10(2)	Mg*A* – O16	2.17
Fe*A* – O16w	2.10(2)	Mg*A* – O16	2.17
Fe1 – O13H	1.92(2)	Fe1 – O13H	2.01
Fe1 – O14w	1.95(2)	Fe1 – O14w	2.08
Fe1 – O12	1.96(1)	Fe1 – O12	2.05
Fe1 – O3	1.99(2)	Fe1 – O3	2.08
Fe1 – O7	2.03(2)	Fe1 – O7	2.00
Fe1 – O15w	2.04(1)	Fe1 – O15w	2.04
Fe2 – O10	1.93(1)	Fe2 – O10	2.00
Fe2 – O13H	1.99(1)	Fe2 – O13H	1.98
Fe2 – O17w	2.06(1)	Fe2 – O17w	2.07
Fe2 – O19w	2.07(2)	Fe2 – O19w	2.10
Fe2 – O1	2.07(1)	Fe2 – O1	2.02
Fe2 – O5	2.08(1)	Fe2 – O5	2.13
S1 – O4	1.46(2)	S1 – O4	1.47
S1 – O2	1.48(1)	S1 – O2	1.48
S1 – O1	1.49(1)	S1 – O1	1.52
S1 – O3	1.49(2)	S1 – O3	1.51
S2 – O7	1.45(2)	S2 – O7	1.51
S2 – O8	1.47(2)	S2 – O8	1.48
S2 – O5	1.48(1)	S2 – O5	1.51
S2 – O6	1.49(1)	S2 – O6	1.48
S3 – O9	1.47(1)	S3 – O9	1.47
S3 – O11	1.47(2)	S3 – O11	1.49
S3 – O12	1.48(1)	S3 – O12	1.51
S3 – O10	1.50(1)	S3 – O10	1.51

* Room-temperature refinement; § *ab initio* results.

TABLE 5. BOND DISTANCES AND BOND ANGLES FOR OXYGEN AND DEUTERIUM ATOMS IN FERRICOPIAPITE* AND OXYGEN AND HYDROGEN ATOMS IN MAGNESIOCOPIAPITE§

ferricopiapite		magnesiocopiapite	
A – *B*	distance (Å)	*A* – *B*	distance (Å)
O13H – D1	0.96(2)	O13H – H1	1.00
O14w – D2	0.97(2)	O14w – H2	0.99
O14w – D3	0.99(2)	O14w – H3	1.00
O15w – D4	0.98(2)	O15w – H4	1.00
O15w – D5	1.00(2)	O15w – H5	1.00
O16w – D6	1.02(3)	O16w – H6	0.99
O16w – D7	1.01(3)	O16w – H7	0.97
O17w – D8	0.99(2)	O17w – H8	0.99
O17w – D9	0.98(2)	O17w – H9	1.01
O18w – D10	0.98(4)	O18w – H10	1.00
O18w – D11	1.03(2)	O18w – H11	1.00
O19w – D12	0.98(2)	O19w – H12	0.99
O19w – D13	0.96(2)	O19w – H13	0.98
O20w – D14	0.99(3)	O20w – H14	0.99
O20w – D15	0.99(3)	O20w – H15	0.99
O21w – D16	0.95(3)	O21w – H16	1.01
O21w – D17	0.98(2)	O21w – H17	0.98
O22w – D18	0.98(2)	O22w – H18	1.00
O22w – D19	0.99(2)	O22w – H19	0.98
O23w – D20	0.99(2)	O23w – H20	0.98
O23w – D21	0.99(2)	O23w – H21	0.98
A – *B* – *C*	angle (°)	*A* – *B* – *C*	angle (°)
D2 – O14w – D3	104.5(1.7)	H2 – O14w – H3	107.4
D7 – O16w – D6	118.9(2.5)	H7 – O16w – H6	104.1
D4 – O15w – D5	106.7(1.5)	H4 – O15w – H5	108.1
D9 – O17w – D8	108.3(1.6)	H9 – O17w – H8	109.0
D10 – O18w – D11	112.6(2.8)	H10 – O18w – H11	107.6
D13 – O19w – D12	109.1(1.8)	H13 – O19w – H12	106.7
D15 – O20w – D14	109.0(2.7)	H15 – O20w – H14	107.1
D16 – O21w – D17	113.6(2.1)	H16 – O21w – H17	104.0
D18 – O22w – D19	111.8(1.9)	H18 – O22w – H19	106.6
D21 – O23w – D20	113.3(2.4)	H21 – O23w – H20	107.4

* Room-temperature refinement; § *ab initio* results.

$\{[A(D_2O)_6](D_2O)_4\}$ (Fig. 4b). The changes are caused by re-orientation of O16w (discussed below), O21w, and O23w. However, the hydrogen bonding of these slabs to the infinite chains is the same as experimentally observed. The local charge (Mg^{2+} or Fe^{3+}) and differences in occupancy of the *A* site thus do not control the general topology of the bonds. As argued above, this is likely due to the spherical charge-density of both HS Fe^{3+} and Mg^{2+}. Therefore, the topology of the hydrogen bonding scheme in ferricopiapite and magnesiocopiapite appears to be very similar. This finding is further corroborated by calculations that were initialized with the final values of the low-temperature Rietveld refinement (Table 1 and S1). During the relaxation, the shape of the unit cell remained fixed, and all internal degrees of freedom were relaxed. The results show that the hydrogen bonding scheme remains unchanged. However, further testing of this hypothesis is currently impossible as the hydrogen-bond scheme in magnesiocopiapite remains unknown.

Coordination of the A site

For the reasons given above, we explored the local coordination of the *A* site by *ab initio* calculations. Where the *A* site is occupied by Mg^{2+}, the calculations indicate six-fold coordination of the *A* site by six H_2O molecules with bond lengths in the range 2.03 – 2.17 Å (Fig. 5a). All hydrogen atoms are oriented outward from the center of the octahedron to participate in the hydrogen bonding with neighboring oxygen atoms.

A detailed analysis of the hydrogen-bonding scheme reveals several differences between theory and experiment. The greatest difference lies in the orientation of the H or D atoms (D6, D7) on the oxygen O16 (Fig. 4). Experimental results indicate a hydrogen bond between D6 and O23w (Table 6), but calculations suggest a hydrogen bond between H6 and O11. Bonding orientation differs also markedly for D7 or H7 (Fig. 4).

To explore these differences in detail, we initialized the relaxation with the structure as obtained from the low-temperature neutron refinement (Table S1). We find that the hydrogen-bonding scheme remained stable and did not revert to another hydrogen-bonding scheme. Therefore, the two hydrogen-bonding schemes correspond to two different minima in configuration space. A comparison of the total energies shows that the

TABLE 6. HYDROGEN-BONDING SCHEME IN FERRICOPIAPITE*

O_{donor}-D···$O_{acceptor}$	distance (Å) O_{donor} – D	distance (Å) D ··· $O_{acceptor}$	distance (Å) O_{donor} – $O_{acceptor}$	angle (°) O_{donor} – D – $O_{acceptor}$
O13H – D1 ··· O22w	0.96(2)	1.80(2)	2.75(2)	172.5(1.4)
O14w – D2 ··· O11	0.97(2)	1.81(2)	2.76(2)	167.3(1.4)
O14w – D3 ··· O2	0.99(2)	1.78(1)	2.76(2)	172.9(1.4)
O15w – D4 ··· O8	0.98(2)	1.58(2)	2.56(2)	172.0(1.4)
O15w – D5 ··· O6	1.00(2)	1.75(2)	2.73(2)	164.8(1.5)
O16w – D6 ··· O23w	1.02(3)	1.61(2)	2.62(3)	168.1(1.9)
O16w – D7 ··· O9	1.01(3)	2.06(3)	2.97(3)	149.9(2.1)
O17w – D8 ··· O8	0.99(2)	1.73(2)	2.72(2)	172.4(1.4)
O17w – D9 ··· O22w	0.98(2)	1.71(2)	2.68(2)	169.8(1.3)
O18w – D10 ··· O21w	0.98(4)	1.79(3)	2.77(3)	171.0(2.8)
O18w – D11 ··· O21w	1.03(2)	1.74(2)	2.74(2)	160.7(2.1)
O19w – D12 ··· O3	0.98(2)	2.10(2)	3.05(2)	160.5(1.4)
O19w – D13 ··· O11	0.96(2)	1.90(2)	2.84(2)	165.6(1.5)
O20w – D14 ··· O9	0.99(3)	1.75(2)	2.74(3)	170.2(2.1)
O20w – D15 ··· O4	0.99(3)	1.82(2)	2.79(2)	167.5(1.9)
O21w – D17 ··· O2	0.98(2)	1.73(2)	2.69(2)	164.8(1.5)
O22w – D18 ··· O6	0.98(2)	1.79(2)	2.75(2)	163.1(1.8)
O22w – D19 ··· O5	0.99(2)	2.18(2)	3.14(2)	163.3(1.4)
O23w – D20 ··· O21w	0.99(2)	2.13(3)	3.10(2)	165.4(1.8)
O23w – D21 ··· O12	0.99(2)	2.15(3)	3.03(2)	147.5(1.7)

* Room-temperature results. No hydrogen bond was found for D16.

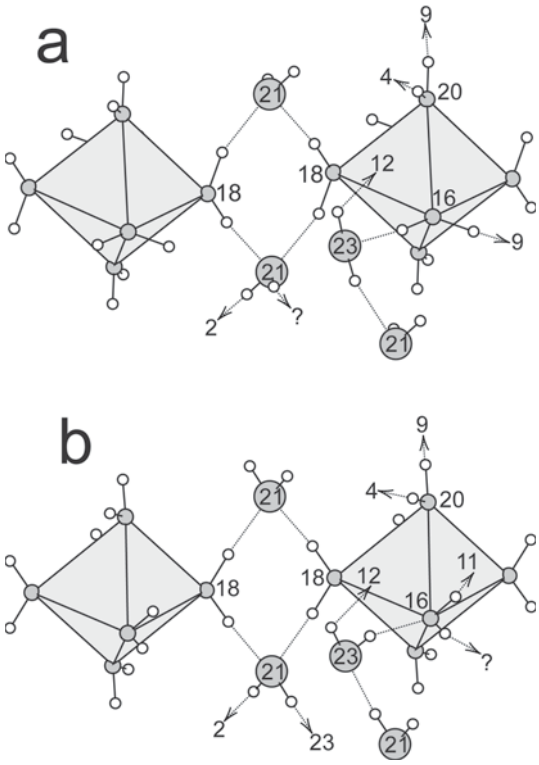

FIG. 4. The hydrogen-bonding schemes among the oxygen atoms near the *A* site: (a) experimentally determined data, (b) data calculated by *ab initio* methods, with the *A* site occupied. Oxygen atoms are the grey spheres, deuterium or hydrogen atoms are the small white spheres; the light grey polyhedra are the $[A(H_2O)_6]$ octahedra. Dashed line segments represent the hydrogen bonds; dashed lines with arrows are hydrogen bonds to the oxygen atoms that belong to the infinite chains. The numbers label the oxygen atoms, either shown in the figure, or the acceptor oxygen atoms in the infinite chains. The dashed line with an arrow and a question mark represent hydrogen atoms with no hydrogen bonds.

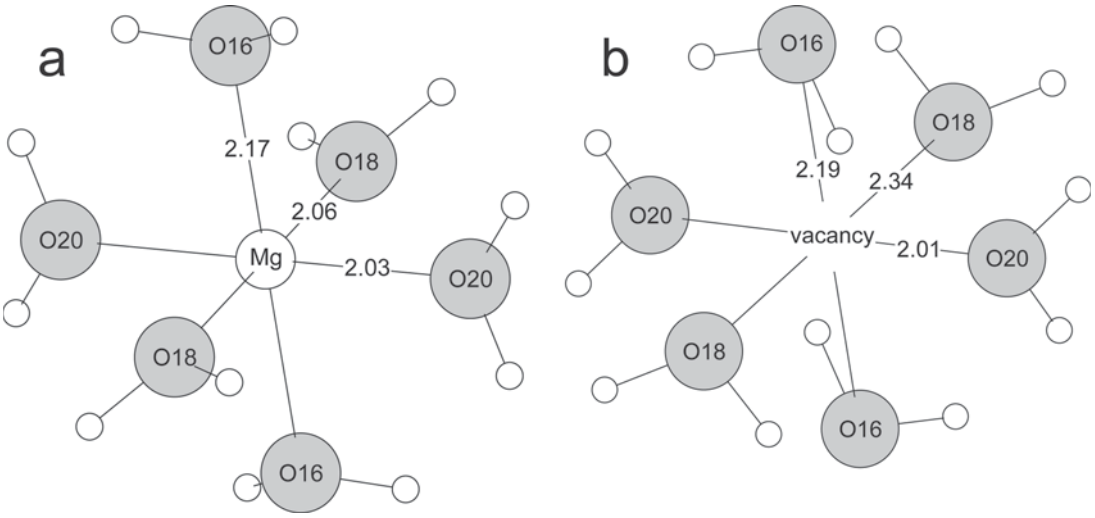

FIG. 5. The local environment of the *A* site (0,0,0), where occupied (a) or vacant (b). The distances shown are the result of the *ab initio* calculation. Note that the center of the octahedron is also an inversion center, and therefore only three center-ligand distances need to be indicated.

structure obtained by relaxing the initial guess of the hydrogen positions is ~0.2 eV/unit cell more favorable and is therefore predicted to be the ground state. We also assessed the robustness of the hydrogen-bonding scheme in the calculated ground-state structure with respect to rotations of the two symmetrically equivalent D6–O16w–D7 molecule. We fixed the intramolecular geometry of the D6–O16w–D7 molecule and rotated the molecule around the O16w–Mg vector. The total energy was then recalculated for a fixed structure and rotation angles between 0° and 360°. No other minimum than the one calculated initially (Table 3, Fig. 4b) was found. The energy for all rotation angles was found to be higher than the ground-state energy, the maximum increase being ~1.7 eV/H_2O molecule. We note that these calculations provide an upper limit for the expected changes in energy, as the structure was not allowed to relax. Nevertheless, the large change in energy associated with the rigid rotation suggests that the arrangement of H_2O or D_2O in copiapite is a cooperative phenomenon that involves several H_2O or D_2O units.

The calculations for the vacant *A*-site show that it is also coordinated by six H_2O molecules (Fig. 5b). However, the H_2O molecules rearrange significantly. This is largely the consequence of the altered charge-balance. Removing Mg^{2+} from the *A* site has two effects: 1) a local charge-deficiency needs to be compensated, and 2) there is an absence of ionic interactions between the central Mg^{2+} and the H_2O molecules. The associated lack of charge transfer from the central cation to the coordinating oxygen ions leads to a coulombic repulsion. The largest changes we observe are associated with the O16w molecule. Smaller changes are observed for O18w, and the environment of O20w remains unchanged (Fig. 4b). This finding is consistent with O20w being hydrogen-bonded to the infinite chains, hindering reorientation of this molecule. The volume of the octahedron increases by 17%, and the hydrogen atoms on O16w and O18w rotate toward the neighboring atoms of oxygen in order to reduce the electrostatic repulsion of the $[H_2O]_6$ octahedron. The presence of vacancies therefore causes significant strain and displacement of O16w and O18w, but even in the extreme case of a completely vacant *A* site, the octahedral arrangement of H_2O molecules is preserved. This remarkable stability of the oxygen arrangement indicates that structural control is independent of the occupancy of this site. A likely controlling factor is hydrogen bonding of O18w and O20w to the infinite chains, even though cooperative and long-range interaction in the H_2O array cannot be ruled out. The vacant *A* sites are the structural units that are most likely able to tolerate a removal of a H_2O molecule. Missing H_2O molecules at these sites could perhaps account for the low H_2O content reported for some samples of copiapite (Zodrow 1980).

The experimental refinement and the *ab initio* calculations converged to an almost identical structural model. This conclusion holds for structural relaxation with variable initial parameters. In particular, the hydrogen-bonding scheme is very similar in experiment and theory. Therefore, the coherency of *ab initio* calculations and experimental results provides insight into the reliability of predicted and refined structural

models, a capability that reaches beyond the potential of each method alone.

Acknowledgements

We are grateful to A.R. Oganov, an anonymous reviewer, U. Kolitsch, and R.F. Martin for careful review and editorial comments of the manuscript. We thank B. Toby and P. Stephens for prompt scheduling and help with experiments at NIST and NSLS, respectively. J.M. appreciates the support that came from the Hess post-doctoral fellowship at the Department of Geosciences at Princeton University. We acknowledge the support of the National Institute of Standards and Technology, U.S. Department of Commerce, in providing the neutron research facilities used in this work. This research was carried out in part at the National Synchrotron Light Source at Brookhaven National Laboratory, which is supported by the US Department of Energy, Division of Materials Sciences and Division of Chemical Sciences. The SUNY X3 beamline at NSLS was previously supported by the Division of Basic Energy Sciences of the US Department of Energy under Grant No. DE–FG02–86ER45231.

References

Atencio, D., Carvalho, F.M.S. & Hypolito, R. (1996): Synthesis and X-ray powder diffraction data for Mg-, Al- and Ni- end-members of the copiapite group. *Anais da Associacao Brasileira de Quimica* **45**, 66-72.

Blöchl, P. E. (1994): Projector augmented-wave method. *Phys. Rev. B* **50**, 17953-17979.

Burns, R.G. (1993): *Mineralogical Applications of Crystal Field Theory.* Cambridge University Press, Cambridge, U.K.

Fanfani, L., Nunzi, A., Zanazzi, P.F. & Zanzari, A.R. (1973): The copiapite problem: the crystal structure of a ferrian copiapite. *Am. Mineral.* **58**, 314-322.

Finger, L.W., Cox, D.E. & Jephcoat, A.P. (1994): A correction for powder diffraction peak asymmetry due to axial divergence. *J. Appl. Crystallogr.* **27**, 892-900.

Hohenberg, P. & Kohn, W. (1964): Inhomogeneous electron gas. *Phys. Rev.* **136**, 864-871.

Jamieson, H.E., Robinson, C., Alpers, C.N., McCleskey, R.B., Nordstrom, D.K. & Peterson, R.C. (2005): Major and trace element composition of copiapite-group minerals and coexisting water from the Richmond mine, Iron Mountain, California. *Chem. Geol.* **215**, 387-405.

Kohn, W. & Sham, L.J. (1965): Self-consistent equations including exchange and correlation effects. *Phys. Rev.* **140**, A1133-A1138.

Kresse, G. & Furthmüller, J. (1996a): Efficiency of *ab-initio* total-energy calculations using a plane-wave basis set. *Comp. Mater. Sci.* **6**, 15-50.

Kresse, G. & Furthmüller, J. (1996b): Efficient iterative schemes for *ab-initio* total-energy calculations using a plane-wave basis set. *Phys. Rev. B* **54**, 11169-11186.

Kresse, G. & Hafner, J. (1993): *Ab-initio* molecular dynamics of liquid metals. *Phys. Rev. B* **47**, 558-561.

Kresse, G. & Joubert, D. (1999): From ultrasoft pseudopotentials to the projector augmented-wave method. *Phys. Rev. B* **59**, 1758-1775.

Larson, A.C. & von Dreele, R.B. (1994): *GSAS. General Structure Analysis System*. LANSCE, MS–H805, Los Alamos, New Mexico.

Libowitzky, E. & Beran, A. (2004): IR spectroscopic characterisation of hydrous species in minerals. *EMU Notes Mineral.* **6**, 227-279.

Majzlan, J., Navrotsky, A., McCleskey, B. & Alpers, C.N. (2006): Thermodynamic properties and crystal structure refinement of rhomboclase, ferricopiapite, coquimbite, and $Fe_2(SO_4)_3(H_2O)_5$. *Eur. J. Mineral.* **18**, 175-186.

Perdew, J.P., Burke, K. & Ernzerhofer, H. (1996): Generalized gradient approach made simple. *Phys. Rev. Lett.* **77**, 3865-3868.

Shannon, R.D. (1976): Revised effective ionic radii and systematic studies of interatomic distances in halides and chalcogenides. *Acta Crystallogr.* **A32**, 751-767.

Stixrude, L. (2002): Talc under tension and compression: spinodal instability, elasticity, and structure. *J. Geophys. Res.* **107**, 2327, doi:10.1029/2001JB001684.

Süsse, P. (1972): Crystal structure and hydrogen bonding of copiapite. *Z. Kristallogr.* **135**, 34-55.

Thompson, P., Cox, D.E. & Hastings, J.B. (1987): Rietveld refinement of Debye–Scherrer synchrotron X-ray data from Al_2O_3. *J. Appl. Crystallogr.* **20**, 79-83.

Zodrow, E.L. (1980): Hydrated sulfates from Sydney coalfield, Cape Breton Island, Nova Scotia, Canada: the copiapite group. *Am. Mineral.* **65**, 961-967.

Received May 31, 2005, revised manuscript accepted January 31, 2006.